Mechanical Systems and Signal Processing 238 (2025) 113229

Contents lists available at ScienceDirect

Mechanical Systems and Signal Processing

journal homepage: www.elsevier.com/locate/ymssp

Full length article

Linear cutting force model to predict battery runtime of jigsaws

Sándor Apáti [a], György Hegedűs [a,*], Sándor Hajdu [b]

[a] Institute of Machine Tools and Mechatronics, University of Miskolc, Miskolc, 3515, Hungary
[b] Department of Electrical Engineering and Mechatronics, Vehicles and Mechatronics Institute, Faculty of Engineering, University of Debrecen, Debrecen, 4028, Hungary

ARTICLE INFO

Communicated by Y. Lei

Keywords:
Sawing performance
Cutting force
Electromechanical model
Scotch yoke mechanism
Linear cutting force
Battery runtime

ABSTRACT

This paper introduces a new linear cutting force model that targets explicitly battery-powered jigsaws, as existing models primarily focus on industrial-scale or CNC-controlled systems. The proposed method uses a basic yet realistic approach to model dynamic force behavior under reciprocating motion instead of previous nonlinear or empirical methods. The model combines the jigsaw's Scotch yoke mechanism with its electrical drive system through MATLAB Simscape to create a coupled electromechanical simulation framework. The model achieves precise experimental runtime data matching through simulated annealing parameter optimization, resulting in only a 3.7% error in runtime prediction. The approach maintains low computational complexity, making it suitable for real-time energy-aware control in handheld tools. The innovation enables longer operation times while minimizing energy consumption and promoting sustainability in mobile construction and maintenance applications.

1. Introduction

The growing use of battery-operated hand tools demands optimization of their system components to achieve better energy efficiency and longer operating time. The performance of power tools depends on multiple variables; yet, cutting forces stand out as essential factors. The forces that develop depend on the tool type, sawing technology, and the physical characteristics of the workpiece material. The reciprocating motion of jigsaws creates special difficulties because they work with different types of materials. The optimization of battery-powered jigsaws' runtime serves both user needs and environmental and economic requirements. Professional and construction operations benefit from extended tool operation because it reduces equipment downtime and decreases battery replacement needs while maintaining continuous work activities. The combination of energy-efficient cutting techniques helps extend tool life while reducing heat damage, supporting sustainability initiatives through reduced energy usage and minimized battery waste. The benefits of these advantages become most important when working in off-grid situations or performing urgent maintenance tasks, as reliable tools with extended autonomy become vital.

1.1. Traditional analytical and mechanistic models

The traditional methods for modeling cutting forces have concentrated on developing physical laws and empirical relationships that describe tool–material interactions. This section reviews fundamental research that established cutting mechanics principles for woodworking through studies of material characteristics, tool shapes, and machining conditions. Traditional approaches to cutting force modeling have focused on establishing physical laws and empirical relationships governing tool–material interaction. This

* Corresponding author.
E-mail address: gyorgy.hegedus@uni-miskolc.hu (G. Hegedűs).

https://doi.org/10.1016/j.ymssp.2025.113229
Received 14 March 2025; Received in revised form 24 July 2025; Accepted 15 August 2025
Available online 27 August 2025

section presents seminal works that laid the foundation for cutting mechanics in woodworking, with a particular focus on material properties, tool geometry, and machining parameters.

Multiple fundamental studies investigated cutting forces by using both analytical modeling techniques and experimental research methods. Ioras et al. Investigated basic cutting mechanics in circular sawing systems by analyzing the connection between cutting forces and process parameters, including feed rate and cutting speed [1]. Their research demonstrated how material properties interact with blade geometry and operational parameters to determine sawing efficiency and accuracy, advancing our understanding of circular sawing process optimization. Porankiewicz et al. investigated the primary and regular cutting forces during machining of various wood species, highlighting how material density and moisture content influence tool wear and cutting resistance [2]. In a subsequent study, they evaluated the effect of feed per tooth and cutting direction on the accuracy of cutting force prediction models, further refining analytical approaches used for circular and band saws [3]. Cristovao et al. presented predictive models for tropical species, accounting for anatomical structure and density [4]. Their regression-based models demonstrated that the anatomical variation of wood species and fiber orientation significantly influenced cutting resistance, thereby helping to refine species-specific toolpath optimization. The study by Germain et al. presents an overview of cutting force modeling techniques from basic mechanistic models to micro-cutting models, with the need to choose appropriate models based on process scales [5]. Their study provided researchers with a guideline to select suitable modeling approaches based on the amount of data and project requirements. Denkena et al. performed an exhaustive analysis of the impact of cutting-edge geometry on machining dynamics in their research [6]. Their research established that particular micro-geometries directly affect the chip formation process and cutting stability, together with surface quality, thus demonstrating the need for proper tool edge design for efficient material removal. Kolar et al. studied how tool wear evolves while quantifying its effects on cutting force coefficients [7]. The experimental findings showed that tool wear progression caused increased cutting resistance and produced unstable force responses, thus demonstrating why precision manufacturing requires continuous tool condition monitoring. Krenke et al. studied the machining process of spruce wood to analyze the relationship between fiber orientation and its impact on cutting forces and surface quality [8]. The study demonstrated how different fiber angles affect tool–material contact, producing quantifiable variations in cutting forces and surface quality. Li et al. performed an experimental study on sawtooth side-edge geometries, which included different radial clearance angles. The researchers proved that side-edge designs optimized for cutting performance decrease both lateral forces and dimensional errors to lengthen tool lifespan and boost machining productivity [9]. The research of Curti et al. resulted in a universal cutting force model for peripheral milling, which includes material density together with chip geometry, grain direction, and tool helix angle to enhance prediction precision in wood machining operations [10]. The research of Torkghashghaei et al. demonstrated that micro-geometry modifications of circular saw cutting edges produce superior surface quality in SPF boards [11]. The research of Jaquemod et al. studied tool temperature and wear behavior under minimum quantity lubrication (MQL) conditions, which resulted in more extended tool durability and reduced energy usage during wood processing operations [12]. The authors of Schreiner et al. performed a Life Cycle Assessment (LCA) to study the environmental effects of circular saw blade production and highlight material and energy conservation during blade life stages [13]. Huang et al. studied the structural alterations of Scots pine through computed tomography scanning. They connected these changes with force variations during sawing to establish a better comprehension of wood behavior during the process [14]. Mandic et al. performed energy-based cutting performance assessments through experimental power measurements at different operational conditions [15]. Moradpour et al. studied the relationship between cutting power and moisture content, as well as feed rate, showing that power response follows nonlinear patterns which affect process planning in moisture-variable environments [16]. Fracture mechanics approaches by Orlowski et al. quantified energy consumption during material separation using shear energy metrics [17], while their subsequent work introduced plasticity-based models incorporating anisotropic failure behavior [18,19]. Hlásková evaluated fracture resistance in solid and thermally modified wood, showing that modification processes reduce cutting resistance and improve machinability [20,21]. Costes et al. developed orthogonal cutting mechanics for hardwood, integrating force analysis with chip morphology characterization [22]. Luo et al. introduced a single-tooth force prediction model using cutting-edge curvature and rake angle as inputs to investigate the effect of the saw tooth profile parameters on the sawing process, to optimize the sawing process [23]. The FRAC_MOD model by Orlowski integrates material deformation, fracture energy, and tool geometry into a unified framework for cutting force prediction [24]. The models were primarily developed for rigid, large-scale setups and did not address handheld tool dynamics.

1.2. Physics-based and numerical models

To better capture complex tool–material interactions, researchers have advanced from analytical to physics-based numerical modeling techniques. These allow for the incorporation of material anisotropy, fracture behavior, and heat transfer mechanisms in force prediction. To better capture complex tool–material interactions, researchers have advanced from analytical to physics-based numerical modeling techniques. These allow for the incorporation of material anisotropy, fracture behavior, and heat transfer mechanisms in force prediction.

Mechanistic and numerical models expanded the analysis to more complex tool–material interactions. Khelifa et al. introduced a material property-based simulation framework for sawing timber, optimizing machining parameters through FEM analysis, and validating the model with experimental data [25]. Marchal et al. applied micromechanical and fracture mechanics principles to wood machining, providing an early conceptual foundation for integrating material anisotropy into predictive models [26]. Naylor et al. developed cutting force models for wood machining based on mechanical properties, incorporating variables such as modulus of elasticity and shear strength [27]. Their models demonstrated improved prediction accuracy for cutting forces under varying material conditions. Conward et al. implemented microstructure-driven simulations for bone sawing, enabling

high-resolution analysis of tissue behavior during cutting and extending their framework to acoustic energy modeling for tool performance assessment [28,29]. Kang et al. formulated a granite sawing model based on the maximum undeformed chip thickness theory, successfully correlating chip morphology with force response and tool load [30]. In thermal–mechanical modeling, Xu presented a coupled thermo-mechanical simulation using ABAQUS, validated against experimental force measurements, to optimize cutting conditions in composite materials [31]. Yu proposed ABAQUS-based simulations incorporating real cutting geometry and temperature feedback for MDF processing [32]. The research of Tan et al. [33] and Ni [34] used Multi-tooth force prediction models and dynamic sawing models to improve tool engagement prediction and sawing efficiency. The models of Vorkapic were integrated into virtual manufacturing environments to achieve better prediction accuracy in manufacturing simulations [35]. For embedded system applications, simple numerical methods were introduced. Pichler employed FEM to optimize the tool geometry to reduce cutting forces and energy consumption in industrial saws [36].

1.3. Data-driven and hybrid modeling approaches

Recent studies have moved beyond physics-based methods by using data-driven and hybrid modeling techniques to address the limitations of purely physics-based methods. Machine learning, together with sensor fusion and real-time feedback systems, is used in these approaches to handle complex nonlinear sawing process behavior better.

Research now increasingly employs data-driven and hybrid modeling techniques to improve the modeling of cutting processes. A high predictive accuracy was obtained by Huang et al. when using machine learning algorithms to predict mechanical properties and milling performance of thermally modified wood through the correlation of process parameters with output quality indicators [37]. Real-time wood density and surface roughness prediction was enhanced by Derbas et al. through the use of sensor fusion techniques that processed vibration, force, and surface data [38]. Lai et al. proposed a hybrid framework for brittle material cutting [39]. This combined method achieved better force prediction accuracy in various tool geometries and feed rate conditions. Sandak et al. designed cutting-force sensors that were installed in saw frames to provide real-time feedback for adaptive process control, which resulted in new tool development [40]. Real-time crack and fiber deviation and instability detection was enabled through vibration-based defect detection schemes introduced by Zhang [41] and Nasir [42]. The sound signals of Thaler et al. were used for chatter phenomenon detection in band sawing to provide real-time non-contact monitoring [43]. Meulenberg et al. studied the evolution of force in Zone II sawing and linked force spikes to tool trajectory and cut initiation [44]. McDonald measured the cutting forces in frozen spruce wood and demonstrated that low temperature intensified resistance through brittle fracture behavior [45]. The cutting force measurement precision of strain gauges developed by Kazup et al. was enhanced especially for dynamic applications [46]. Blokhin et al. studied the suppression of resonance in sawing tools through real-time feedback to reduce excessive vibration and increase tool lifespan [47]. Marega et al. presented a saw blade monitoring system with integrated sensors to enhance cutting stability and showed the possibility of embedding intelligent feedback in industrial saws [48]. Zhang et al. used AI technology to develop tools for wear monitoring and thermomechanical modeling during wire sawing of brittle materials [49]. The findings of their research support the integration of temperature-sensitive modeling and tool state tracking for handheld tools despite their different application area. Yu et al. proposed the use of LSTM digital twins for tool condition monitoring, which can be integrated with Jigsaw platforms in the future [50]. Sun et al. used reinforcement learning to control force trajectories in intelligent milling that provides a theoretical basis for future jigsaw motion optimization [51]. The Derbas et al. sensor fusion system combined airborne sound, cutting forces, power consumption, and acoustic emissions for milling various wood-based products [52].

Data-driven modeling techniques have not been successfully applied to handheld reciprocating tools, including jigsaws. The generalization is limited by sensor resolution restrictions, together with high-frequency real-world data noise and jigsaw motion modeling difficulties stemming from rapid direction changes and acceleration transients. The computational constraints of portable devices make the implementation of real-time predictive models more difficult.

1.4. Comparison with other sawing technologies

Handheld jigsaws differ significantly from circular saws, band saws, and wire saws in terms of their operational characteristics and modeling challenges, despite extensive research on these three types of saws. Circular saws used in woodworking and metal cutting operations use a rotating disk and perform continuous unidirectional motion. The quasi-stationary nature of their dynamics allows for stable cutting force models that depend on material removal rate and blade geometry. The continuous loop blade of band saws makes them suitable for contour cutting while providing smoother operation with reduced vibration levels than jigsaws. Wire saws that use flexible wire under tension and abrasive action are used in semiconductor and stone processing and exhibit low cutting forces while delivering high precision (see Fig. 1).

Jigsaws operate as lightweight, battery-powered handheld tools that provide flexible operation in off-grid construction, renovation, and maintenance tasks. The reciprocating motion of these tools produces high-frequency accelerations and directional reversals, which lead to significant force variations and transient behavior. Unlike the above-mentioned sawing technologies, jigsaws require models that can cope with irregular tool–material contact, rapidly changing dynamics, and constrained computational resources. Table 1 summarizes the key distinctions between these saw types. The comparisons reveal how modeling jigsaws remain innovative due to their portable nature, electromechanical coupling, and dynamic motion, which create unique problems that standard stationary tool models cannot solve. The research fills the existing knowledge gap through a simple yet meaningful model that addresses the specific characteristics of handheld sawing operations.

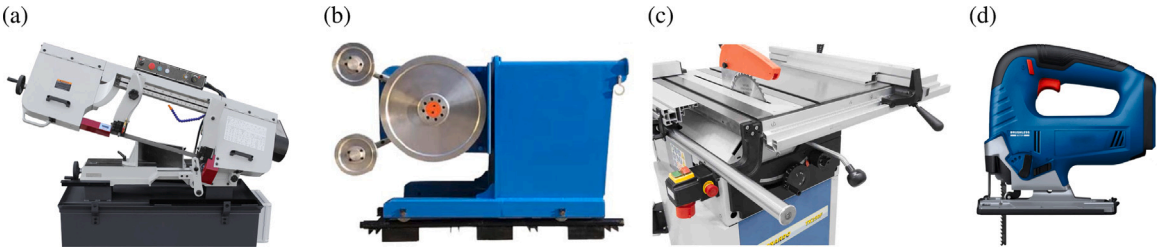

Fig. 1. Different sawing machines. (a) Band sawing machine; (b) Wire sawing machine; (c) Circular table sawing machine; (d) Handheld jigsaw powertool.

Table 1
Comparison of different sawing technologies.

Saw type	Motion type	Typical use	Power supply	Modeling complexity
Circular saw	Rotational	Wood, metal cutting	Grid power	Moderate
Band saw	Continuous loop	Wood, metal cutting	Grid power	Moderate
Wire saw	Flexible wire under tension	Stone cutting	Grid power	Low
Jigsaw	Reciprocating	Wood, metal cutting	Battery-powered	High

1.5. Identified research gap and present work

The literature review shows major progress in sawing force modeling, especially for industrial-scale applications. Research on handheld reciprocating tools, including jigsaws, has received insufficient attention in the scientific literature. The operating conditions of these tools include fast reversing cutting motions together with changing blade-material contacts and major acceleration–deceleration patterns. The existing cutting force models, which are nonlinear or empirically fitted, fail to model transient and asymmetric systems because they assume quasi-stationary motion with uniform material removal.

This research presents a new linear cutting force model that addresses the distinctive motion characteristics of handheld jigsaws. The proposed linear model represents a unique approach because it unites mechanical damping principles with electromechanical coupling through the Scotch yoke mechanism. The linear model structure provides fast computational performance while retaining the fundamental dynamic characteristics of the jigsaw system. The model enables real-time battery runtime prediction and energy-conscious control operations on embedded systems that have restricted processing capabilities.

Unlike nonlinear cutting models that require iterative numerical solvers and multi-parameter identification routines — often impractical for portable tools — the proposed model minimizes complexity by relying on physically interpretable parameters and global optimization using simulated annealing. It stands apart from existing methods by avoiding empirical look-up tables or material-specific calibration, yet still achieving a runtime estimation error of only 3.7% relative to experimental measurements.

This balance between accuracy and simplicity is particularly valuable for consumer and professional applications where predictive runtime, thermal safety, and tool efficiency are critical but onboard computation is constrained. Thus, the model offers a previously unavailable solution for the simulation-driven design and control of battery-powered reciprocating saws.

The following sections of this article are organized as follows: Section 2 presents the experimental setup. Section 3 describes the dynamic model. Section 4 discusses force modeling and battery simulation. Section 5 reports results, followed by conclusions in Section 6.

2. The in-situ measurement system of cutting force

The experimental system consists of a jigsaw equipped with force and inductive sensors to analyze real-time cutting forces. The setup includes a data acquisition system that records the signals during cutting tests on different wood types. The goal is to evaluate the impact of material properties and cutting parameters on the forces acting on the tool (see Fig. 2). The measurement aims to thoroughly examine and optimize the jigsaw's cutting process, with a particular focus on modeling the cutting force and the efficient use of the battery. The first step is determining the actual cutting force under various machining conditions, providing essential information about the tool's power requirements and energy consumption [53]. Subsequently, linear and nonlinear models are developed based on the measured data to simulate the jigsaw's behavior under different cutting conditions. The linear model offers a simplified approximation for describing the cutting force and motor current's behavior, while the nonlinear model provides dynamics closer to reality. For model refinement, a parameter identification process is applied, during which the damping factor of the linear model is optimized based on comparisons with real measurements. The resulting linear model not only enables fast simulations but also provides reliable estimates of battery runtime. The MATLAB/Simscape environment is used for simulations, which allows for integrated modeling of the electromechanical system's physical parameters and control strategies. The aim was to create a computationally efficient yet reliable linear model that closely approximates the actual cutting force and current consumption. The resulting model and findings contribute to improved jigsaw operation, particularly concerning battery life and energy consumption.

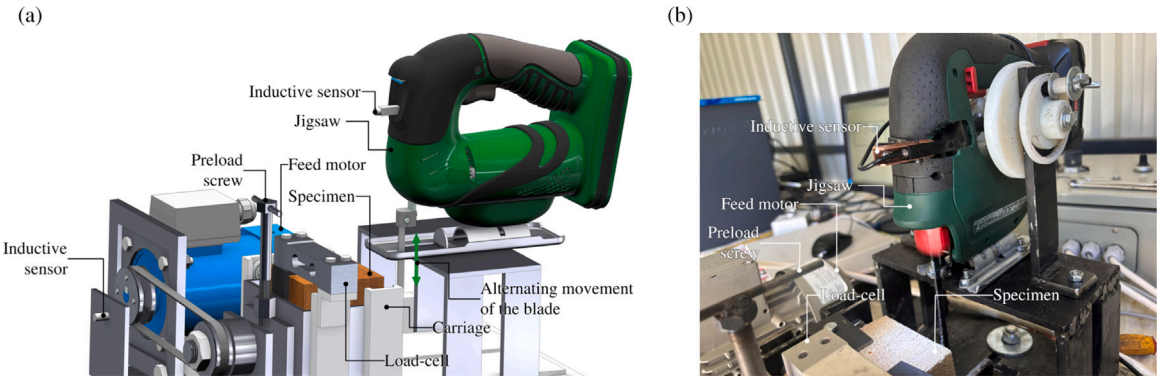

Fig. 2. Measuring system for cutting force measurement with jigsaw. (a) Conceptional assembly model and arrangement of test bench; (b) Physical measurement arrangement.

Table 2
Material properties of investigated workpieces.

Property	Nylon 6 (PA 6)	European black locust	White Oak
Density [g/cm^3]	1.14	0.68	0.68
Hardness, Wood indentation [N]	–	7500	6050
Hardness, Rockwell M	85	–	–
Elastic or flexural modulus [GPa]	2.5	11.07 (flexural)	12.3 (elastic)
Tensile strength [MPa]	67	133[a]	5.52[a]
Homogeneity	Homogeneous	Less homogeneous	Less homogeneous

[a] Perpendicular to grain.

The arrangement of the test equipment is shown in Fig. 2(b). The test specimen is placed in a specially designed carriage system for cutting experiments, which can only move vertically. Rolling bearings reduce friction and ensure smooth, unobstructed movement of the carriage, guided slides ensure the rigidity of the equipment. The structure is designed so the carriage can only move along the cutting force's line of action. A load cell is attached to the carriage, continuously measuring the force exerted in the cutting process and providing an output signal proportional to the values. This load cell is one of the most critical components of the test bench, as it accurately monitors the cutting process.

In the course of the design, special attention was paid to minimizing unwanted vibrations, as they could distort measurements, reducing system accuracy. To this end, the carriage system was equipped with a preloaded threaded spindle that exerts a constant force F_c in the resting position between the carriage and the load cell. This preload stabilizes the carriage, improving measurement accuracy, and reducing the impact of vibrations.

2.1. Cutting force measurement on different workpiece materials

During the experiments, the cutting forces were analyzed for three different materials: Nylon 6 (PA 6), European black locust (acacia) wood, and White oak wood. The aim of the analysis was to understand how material density, hardness, and mechanical properties affect cutting forces and machining dynamics. The properties of the materials are summarized in Table 2 (source: www.matweb.com).

The table provides a detailed overview of key material properties affecting the cutting process. Nylon 6 (PA 6) is a homogeneous engineering plastic with consistent mechanical and physical characteristics, which leads to reduced cutting force fluctuations and more stable machining conditions. In contrast, the fibrous and inhomogeneous structure of acacia and oak results in higher cutting force variability. This structural inhomogeneity significantly influences cutting dynamics and poses challenges for precision machining.

To ensure the validity of the measurement results, the impact of tool wear was considered during testing. Each measurement series — defined by a unique combination of material type and parameter settings — was initiated with a new jigsaw blade to maintain consistent cutting edge conditions. Each series consisted of three repetitions, during which the blade condition was visually inspected. If signs of tooth rounding or deformation were detected, or if the specific cutting force increased by more than 20%, the blade was replaced. Although no explicit wear model was applied, this protocol minimized tool-wear-related distortions and ensured reliable and comparable cutting force data.

Nylon 6 (PA 6), being a lightweight engineering plastic with relatively low stiffness, requires less cutting force during machining. Its good mechanical resistance and low density also contribute to improved energy efficiency in cutting applications.

In wood materials, the fibrous structure introduces higher variability in cutting forces, making it more difficult to determine optimal cutting parameters. However, this natural inhomogeneity contributes to the unique behavior of wood, which can be

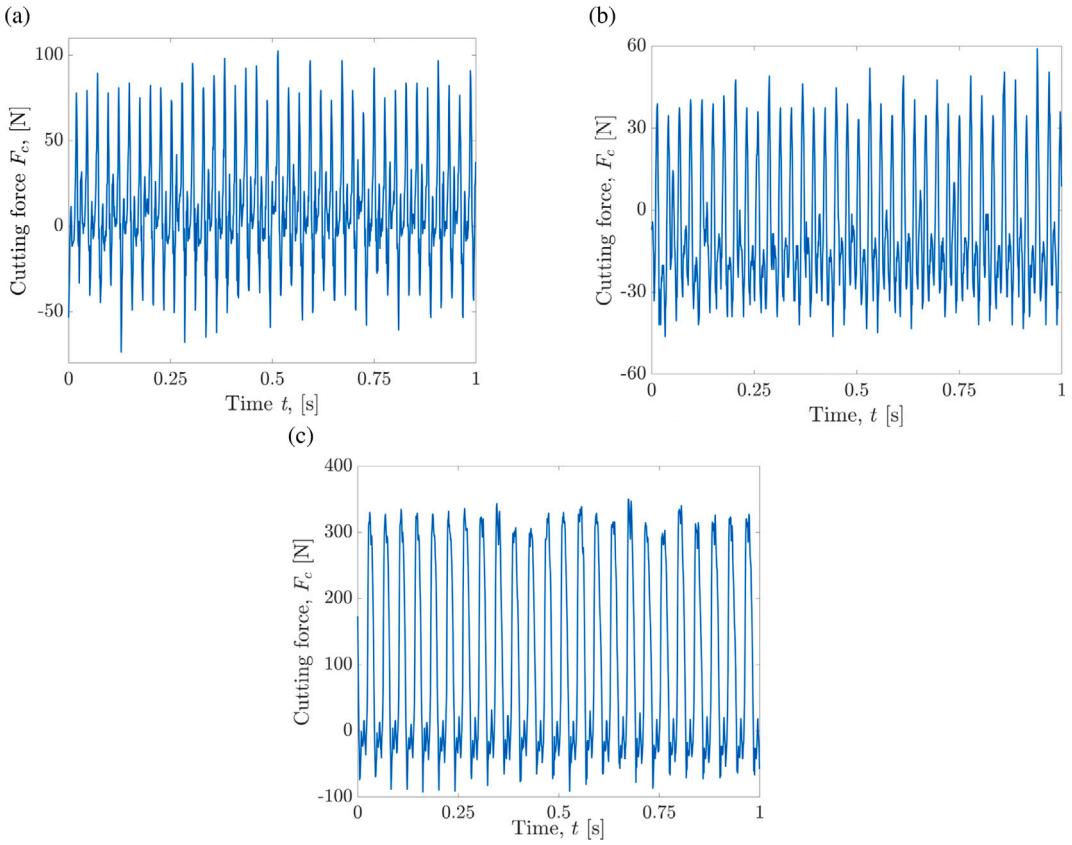

Fig. 3. Measured cutting forces on different workpiece materials. (a) European black locust (Acacia) wood; (b) Nylon 6 (PA 6); (c) White oak wood.

leveraged in practical applications. Based on the collected data, cutting parameters for handheld jigsaws — such as blade speed and feed rate — can be optimized to enhance both cutting efficiency and tool longevity.

The results showed significant differences in cutting force behavior, as illustrated in Fig. 3. Fig. 3a presents the cutting force diagram for black locust. The high force amplitudes observed in white oak were mainly due to its dense, fibrous structure, which leads to non-uniform resistance and fluctuating force values (Fig. 3c). In contrast, Nylon 6 (PA 6) exhibited lower stable cutting forces, typically peaking around 60 N (see Fig. 3b). These differences stem from its homogeneous composition, which provides uniform material removal conditions.

3. Dynamic model of scotch yoke mechanism

In this section, the electromechanical model of the driving mechanism is presented. This model aims to accurately describe the motion and dynamic behavior of a handheld jigsaw mechanism, enabling the analysis of both mechanical and electrical effects during the cutting process. By defining the theoretical foundations and preparing simulations, the model facilitates the investigation of various cutting conditions, the impact of cutting forces, and the prediction of the system's response. The Scotch yoke mechanism performs the conversion of rotary motion to linear motion, with a particular focus on mechanical energy transmission. This type of mechanism is widely used as an ordinary motion conversion mechanism and as unique amplitude modulation pinion mechanisms or elements of a vibration isolator system [54,55]. Fig. 4(b) shows the dynamic model of the Scotch yoke mechanism driven by a permanent magnet DC motor. The motor is connected via a gear driving mechanism to the sliding pin, which produces the oscillatory, i.e., alternating, motion of the saw blade, thereby providing the back-and-forth movement necessary for sawing. The following equation determines the blade's position, which describes the current position of the saw blade based on the crank radius and the angular displacement:

$$y(t) = r_c \left(1 - \cos \varphi_c\right), \tag{1}$$

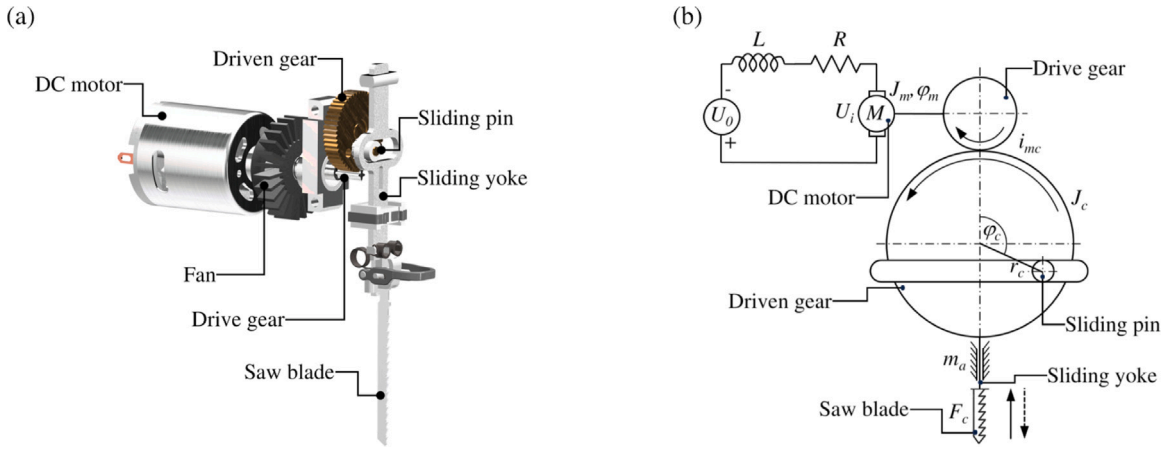

Fig. 4. Electromechanical model of the jigsaw driving mechanism. (a) Main components of driving mechanism with DC motor and Scotch yoke mechanism; (b) Main design parameters — electrical and mechanical — of electromechanical model of driving mechanism.

where $y(t)$ is the blade position, r_c is the crank radius, and φ_c is the angular displacement of the crank wheel. The relationship between the motor shaft angular displacement and the crank wheel angular displacement is determined by the gear ratio i_{mc}:

$$\varphi_m = i_{mc}\varphi_c, \tag{2}$$

where φ_m is the motor angular displacement. The time derivative of Eq. (1) provides the velocity function of the saw:

$$\dot{y}(t) = r_c\dot{\varphi}_k \sin\varphi_c, \tag{3}$$

where $\dot{\varphi}_c$ is the angular velocity of the Scotch yoke wheel. The mathematical model of the jigsaw is constructed using an energy-based approach, employing displacement and charge as variables. For this purpose, the Lagrangian L_f is formulated based on conservative components of the system, incorporating the kinetic co-energy T^* and the magnetic co-energy W_m^* of the coil. Based on Fig. 4(b), the Lagrangian, incorporating the energies stored in the conservative components, is given as:

$$L_f = T^* + W_m^* = \frac{1}{2}\left(J_m\dot{\varphi}_m^2 + J_c\dot{\varphi}_c^2 + m_a\dot{x}^2 + L\dot{q}^2\right), \tag{4}$$

where J_m is the moment of inertia of the motor shaft, J_c is the moment of inertia of the Scotch yoke wheel, m_a is the mass of the alternating Scotch yoke mechanism, L is the inductance of the coil and $\dot{q}$ is the time derivative of charge, representing current. The reciprocal of the gear ratio $k_{mc} = \frac{1}{i_{mc}}$ allows the reduction of variables when substituted in Eqs. (2) and (4):

$$L_f = \frac{1}{2}\left[\left(J_m + J_c k_{mc}^2 + m_a r_c^2 k_{mc}^2 \sin\left(k_{mc}\varphi_m\right)\right)\dot{\varphi}_m^2 + L\dot{q}^2\right]. \tag{5}$$

Defining the reduced moment of inertia of the system as follows:

$$J_r\left(\varphi_m\right) = \left[J_m + J_c k_{mc}^2 + m_a r_c^2 k_{mc}^2 \sin\left(k_{mc}\varphi_m\right)\right]. \tag{6}$$

The Lagrangian can be expressed as

$$L_f = \frac{1}{2}\left[J_r\left(\varphi_m\right)\dot{\varphi}_m^2 + L\dot{q}^2\right]. \tag{7}$$

For the non-conservative components shown in Fig. 4(b), the virtual work can be written as:

$$\delta W_{nc} = \delta q\left(U_0 - R\dot{q} - k_e\dot{\phi}_m\right) + \delta\phi_m\left(k_m\dot{q} - F_c r_c k_{mc}\sin(k_{mc}\phi_m) - b\dot{\phi}_m\right), \tag{8}$$

where δW_{nc} is the virtual work of the non-conservative components, U_0 is the terminal voltage, δq is the virtual change in charge, R is the circuit resistance, k_e is the electrical constant of the motor, $\delta\varphi_m$ is the virtual change in the angular displacement, F_c is the cutting force and b is the internal damping coefficient of the motor. For upward movement, the saw cuts, while in the course of downward motion, due to a blade-tilting mechanism, no cutting force occurs, as reflected in Eq. (8):

$$F_c = \begin{cases} F_c(\varphi_c), & \text{if } sin(\varphi_c) > 0, \\ 0, & \text{if } sin(\varphi_c) \le 0. \end{cases} \tag{9}$$

Using the generalized coordinates q and φ_m, the Lagrangian and virtual work yield the following Lagrange equations of motion:

$$\frac{d}{dt}\left(\frac{\partial L_f}{\partial\dot{q}}\right) - \frac{\partial L_f}{\partial q} = U_0 - R\dot{q} - k_e\dot{\varphi}_m, \tag{10}$$

Table 3
Main parameters of the electromechanical system.

Input parameters	Value	Unit
R - circuit resistance	0.176	Ω
L - coil inductance	$3.21 \cdot 10^{-3}$	H
k_e - motor electric constant	$7.383 \cdot 10^{-3}$	V s rad^{-1}
k_{mc} - reciprocal of the gear ratio	6/56	–
J_m - moment of inertia of DC motor	$2.4 \cdot 10^{-5}$	kg m^2
k_m - motor torque constant	$5.632 \cdot 10^{-6}$	N m A^{-1}
J_c - moment of inertia of Yoke wheel	$2.38 \cdot 10^{-5}$	kg m^2
m_a - mass of moving components	0.239	kg
r_c - crank radius	0.01	m
b - internal damping coefficient	$3.4274 \cdot 10^{-6}$	N m s rad^{-1}
U_0 - battery voltage	18	V

$$\frac{d}{dt}\left(\frac{\partial L_f}{\partial \dot{\varphi}_m}\right) - \frac{\partial L_f}{\partial \varphi_m} = k_m \dot{q} - F_c r_c k_{mc} \sin\left(k_{mc}\varphi_m\right) - b\dot{\varphi}_m. \tag{11}$$

From Eqs. (7) and (8), the electromechanical differential equations are derived:

$$L\ddot{q} + R\dot{q} + k_e\dot{\varphi}_m = U_0, \tag{12}$$

$$J_r(\phi_m)\ddot{\phi}_m + \frac{1}{2}J_{r'}(\phi_m)\dot{\phi}_m^2 = k_m\dot{q} - F_c r_c k_{mc}\sin(k_m k\phi_m) - b\dot{\phi}_m. \tag{13}$$

The mechanical equation is highly non-linear, as its coefficients are not constants and contain the square of $\dot{\varphi}_m$. Moreover, the cutting force is a function of φ_m. The above-defined mathematical problem can be numerically solved in several software environments. In this study MATLAB/Simscape was applied to produce the solutions. The simulation parameters for the electromechanical model of the jigsaw are presented in Table 3, where the equipment technical data and component geometries determine the values.

4. Dynamic simulation of sawing process

This section describes the modeling of dynamic simulation of the cutting process and battery runtime using Simscape software. This advanced simulation environment allows for realistic modeling and analysis of physical systems, such as electromechanical systems. In electromechanical modeling, integrating electrical and mechanical components into the model accurately represents the system's dynamics. Built-in libraries can use motors, dampers, springs, and various electrical elements such as resistors, inductors, and capacitors when modeled electromechanical systems. These elements can be parameterized based on physical properties such as electromotive force (EMF), resistance, inertia, and damping. Electrical and mechanical elements can be interconnected through specialized blocks, enabling an accurate simulation of mechanical systems [56,57]. This allows one to examine the system responses, such as time-dependent variations of current consumption, voltage, speed, and torque under different load conditions. Optimization options like simulation can fine-tune parameters to match real-world conditions. Direct integration with Simulink provides an opportunity to incorporate control algorithms and logic, enabling simulation of the system's physical dynamics and control strategies. Simscape models can be directly linked to the Simulink environment, combining physical models with control logic and providing additional flexibility in system development and testing.

4.1. Preparation of measured cutting force for simulation

The cutting force-time diagram measured on an actual jigsaw is shown in Fig. 5(a), which is the basis for the simulation model. The measurement setup and arrangement is described in detail in Section 2. The cutting force-time function depicted reflects the force variations in the oscillating motion of the jigsaw, representing the dynamic interactions between the tool and the workpiece. As shown, the measurement duration was 1 s. For simulation purposes, the cutting force-time data must be transformed into a cutting force-angular displacement function. This transformation enables the cutting force to be represented as a periodic function based on the blade's angular position, accurately reflecting the forward and backward cycles of the jigsaw. Mapping according to angular displacement ensures that realistic force effects are represented in the course of simulation, enabling more precise modeling and analysis of the system. To derive the cutting force-angular displacement function from the cutting force-time function, a single period representing one full oscillation cycle of the jigsaw is selected. This can be efficiently achieved using Fourier analysis of the force data. The selected period is assigned to the angular range 0 to 2π, representing the complete motion cycle based on the angular position of the Scotch Yoke mechanism. The cutting force corresponding to each angular position is denoted as $F(\varphi_c)$, where φ_c is the crank angular displacement. Since the blade cuts only in the course of the upward motion due to the tilting mechanism, the cutting force is considered zero in the $0 - \pi$ angular range. As shown in Fig. 5(a), some force effects arise in the course of these periods due to dynamic effects, but they are neglected and set to zero in the course of data reprocessing, the processed data are shown in Fig. 5(b).

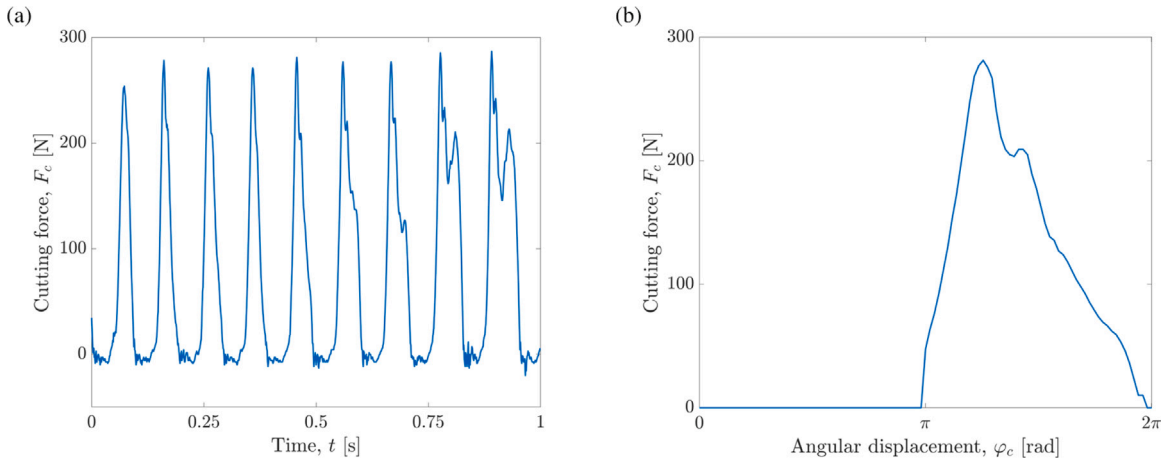

Fig. 5. Typical properties of the cutting mechanism. (a) Measured cutting force during a sawing process, peak value of cutting force F_c = 287.11 N; (b) Cutting force as a function of angular displacement: no cutting during forward movement (F_c = 0 N).

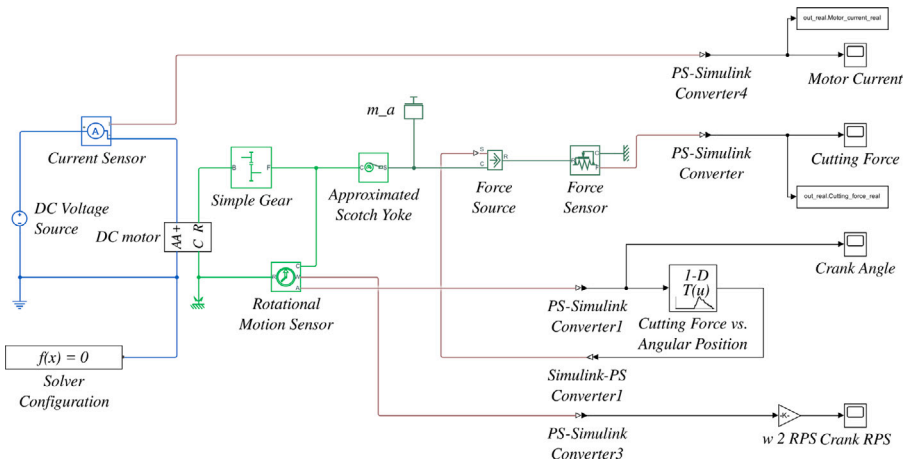

Fig. 6. Simscape model with real cutting force.

4.1.1. Modeling of real cutting force

The electromechanical model of a jigsaw, developed in the Simscape environment for realistic system simulation is presented in Fig. 6. The model connections are color-coded to indicate the types of physical signals and interactions. The blue lines represent electrical signals and energy flow, the light green lines represent rotational mechanical motion, the dark green lines represent translational mechanical effects, and the orange lines represent general Simscape data flow. Black connections represent abstract Simulink data flow. These color codes help you quickly identify connections between different physical domains. The central component of the model is a direct current (*DC*) motor, which converts electrical energy into rotary motion. This rotary motion is transmitted through a gear mechanism to a Scotch yoke system, generating the oscillating motion responsible for the cyclic forward and backward movement of the saw blade. The m_a block represents the alternating mass, which is connected to the stationary environment through the cutting force generating element (*Force Source*) and a force sensor. The input to the *Force Source* block is generated by an *1-D Lookup Table* (*Cutting Force vs. Angular Position* block) that contains the function described in Section 4.1. This block calculates the instantaneous cutting force value from the angular position of the crank. The model utilizes several sensors to accurately monitor the dynamic behavior. The current sensor measures motor current, the rotational motion sensor tracks the angular position and velocity of the crank mechanism, and the force sensor measures forces in the course of cutting. These data allow for a detailed analysis of system behavior and a precise simulation of the cutting force dynamics. This comprehensive structure ensures that the model faithfully reflects not only the physical processes but also all essential aspects of the cutting operation, including dynamic behavior, energy efficiency, and mechanical stability.

4.1.2. Modeling of DC motor

The Simscape DC motor model shown in Fig. 7 shows the drive motor of the jigsaw, which is crucial to simulating the operation of the electromechanical system.

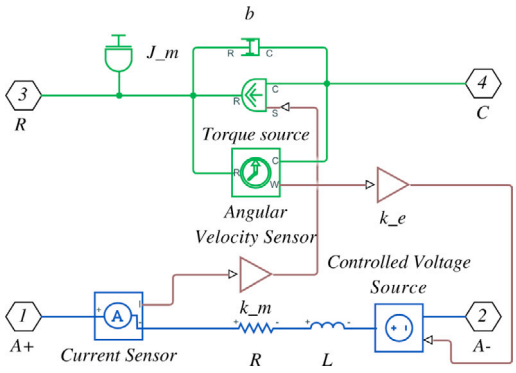

Fig. 7. Block diagram of the DC motor.

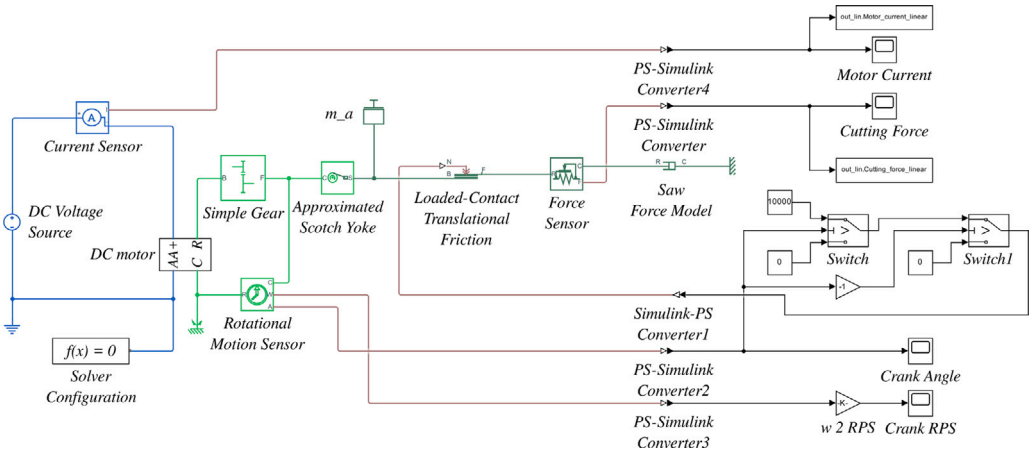

Fig. 8. Simscape model with a linear cutting force model.

The model is built on a precise configuration of electrical and mechanical parameters to accurately replicate the real motor. In the model, the electrical properties of the motor are defined by the resistance parameters R_a, the inductance L and the electromotive force (*EMF*). Equation *EMF* is proportional to the speed of the motor, allowing the model to account for changes in voltage and current at different motor speeds. This effect is created by the *Controlled Voltage Source* block in the model. The motor voltage input is connected in the Simscape circuit in a manner similar to the real system, allowing an accurate representation of current consumption and output torque variations. In the mechanical section, the inertia of the rotor J_m and the damping b are also specified, which influence the motor response time and dynamic behavior. The J_m inertia block describes the rotating inertia effect of the motor, while the damping b models the mechanical resistance that reflects energy losses in the course of motion. These parameters ensure that the motor reacts realistically to load changes in the system. The *Torque Source* block produces the torque dependent on the armature current generated by the motor.

4.1.3. Modeling a linear cutting force approximation

The model shown in Fig. 8 demonstrates the simulation of the jigsaw electromechanical system, designed with a particular focus on the modeling of the cutting force based on linear approximation.

The goal of the model is to accurately represent the sawing process, while enabling faster analysis with simplified calculations that still yield realistic results. Similarly to the model in Fig. 6, the primary energy source of the system is a *DC Voltage Source* block, which supplies power to the DC motor and provides the electrical energy required for the entire model. The DC motor converts electrical energy into rotational mechanical motion, which is transmitted via a simple gear mechanism to the Scotch yoke system. This mechanism transforms rotational motion into oscillatory motion, which is essential for the back-and-forth movement of the saw blade, driving the sawing process. The model includes a linearized cutting force model that calculates the cutting force as a function of the speed and resistance of the blade. The component *Saw Force Model* (actually a linear damper) is responsible for modeling this simplified behavior, while the block *Loaded-Contact Translational Friction* performs the damper operation by connecting it to the stationary environment at the appropriate time. These elements ensure a realistic simulation of the system dynamics while increasing computational efficiency. The series-connected logic switches (*Switch* blocks) are used to control the system operation, providing a normal force to the friction block over the appropriate range of crank angle. The key components of the system include a

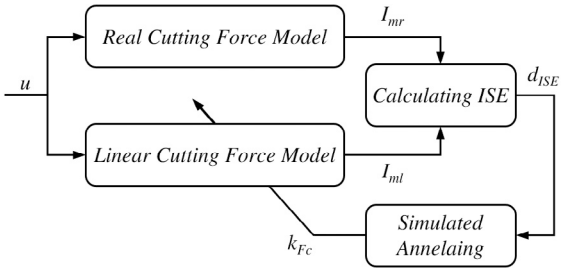

Fig. 9. Real and linear cutting force model optimization via simulated annealing algorithm.

current sensor (*Current Sensor*) that measures motor current consumption and a rotational motion sensor (*Rotational Motion Sensor*) that tracks the rotational motion of the crank mechanism, including the angular position and velocity. These sensors provide critical data for analyzing the cutting process, such as cutting force, motor energy consumption, and dynamic behavior. The output signals include the time-dependent variations of the cutting force and motor current consumption, provided in formats suitable for data analysis and visualization (e.g., Simulink-compatible data). The angular position and speed of the crank mechanism are also part of the output information, reflecting the precise relationship between motion and force effects. This model thoroughly analyzes the dynamic effects that occur in the course of the sawing process, while effectively reducing computational demand through a linear approximation. This model not only simulates the mechanical and electrical components, but also enables a precise analysis of energy consumption and cutting efficiency. Due to its flexibility and optimization capabilities, the model is an ideal tool for analyzing the operation of the jigsaw, particularly in terms of improving energy efficiency, cutting quality, and system stability. As such, it provides relevant results not only for research purposes but also for industrial applications.

4.2. Linear damping factor of cutting force approximation

The parameter of the linear cutting force model is determined by parameter identification based on optimization, with the aim of finding a damping factor (k_{Fc}) that minimizes the discrepancy between the current functions of the real and simulated motor. The real motor current-time function is denoted by $I_{mr}(t)$, while the linear model's current-time function is denoted by $I_{ml}(t)$. The objective is to minimize the discrepancy between these two functions by finding an optimal k_{Fc}. The cost function to minimize is the integral of squared errors (d_{ISE}), which integrates the squared differences between the current-time functions in the time domain:

$$d_{ISE} = \int_0^T \left(I_{mr}(t) - I_{ml}(t)\right)^2 dt. \tag{14}$$

This cost function ensures that the linear model's current-time function closely matches the real measurements. In the integral Eq. (14), each instantaneous discrepancy is squared, giving greater weight to larger errors and significantly influencing optimization. For numerical simulation, discrete time points are used instead of continuous time t. The integral is approximated as a finite sum expressed as:

$$d_{ISE} \approx \sum_{n=1}^{N} \left(I_{mr}(n) - I_{ml}(n)\right)^2. \tag{15}$$

Here, N is the number of discrete time points, and $I_{mr}(n)$ and $I_{ml}(n)$ represent the values of the real and simulated motor current at time t_n. The discrete value d_{ISE} estimates the total discrepancy throughout the simulation period by summing the differences at individual time points. The goal is to minimize this cost function by selecting an optimal k_{Fc} that best aligns the motor current-time function of the linear model with the real measurements. To find the optimal k_{Fc}, the simulated annealing algorithm is used. Simulated annealing is a metaheuristic optimization method designed to achieve global minima in combinatorial and continuous optimization problems. For the design and optimization of unit tandem mechanisms with multiple closed loops, an improved simulated annealing-greedy algorithm is proposed. This algorithm efficiently filters out optimal design solutions to solve the challenging problem of handling a large number of configurations. This developed software platform, which enables automated synthesis filtering tasks, is also suitable for mechanism design tasks [58].

In the course of the process, the parameter k_{Fc} is modified iteratively, recalculating d_{ISE} at each step. A new parameter value is accepted if it decreases d_{ISE}, otherwise it can still be accepted randomly to avoid local minima. This procedure ensures that the linear model aligns as closely as possible with real measurement data, providing the most accurate estimate for cutting force simulation. Fig. 9 summarizes the results of determining the optimal damping factor and predicting the battery runtime for the real and linear cutting force models. The identification block diagram consists of two main components: the real cutting force model and the linear damping factor-based cutting force model. The motor current-time functions of the two models are compared, and the integral of squared errors (*ISE*) measures the discrepancy, minimized to find the optimal damping factor. According to block diagram logic, the optimization continuously compares the results of the real and linear models using the *Simulated Annealing* algorithm, which iteratively searches for a damping factor that minimizes the discrepancy between the two models. The optimization aims to align the linear model with the behavior of the real cutting force, ensuring simulation accuracy.

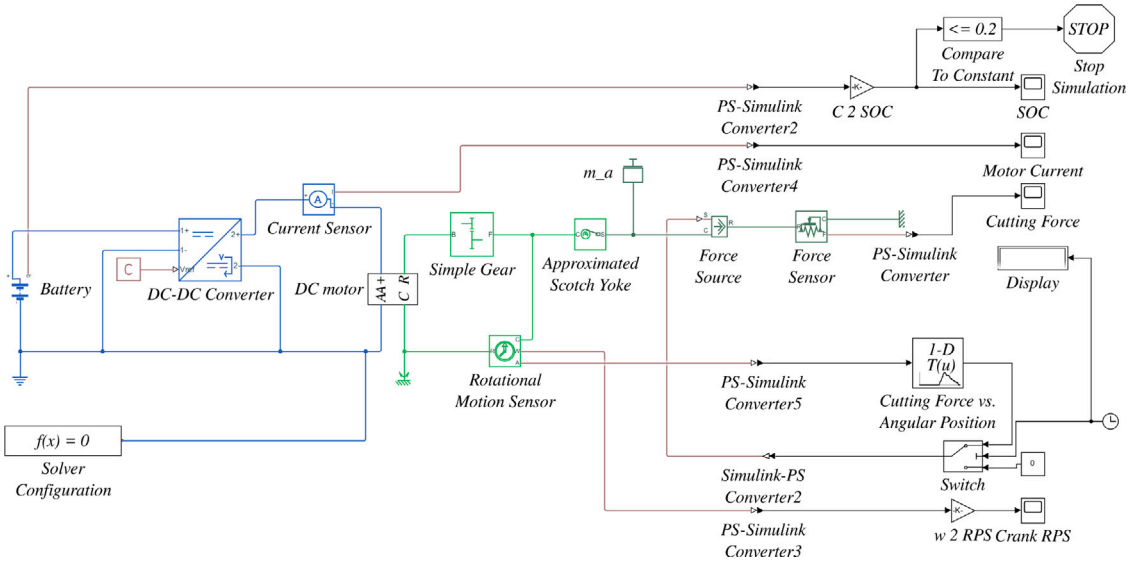

Fig. 10. Battery runtime simulation with real cutting force model.

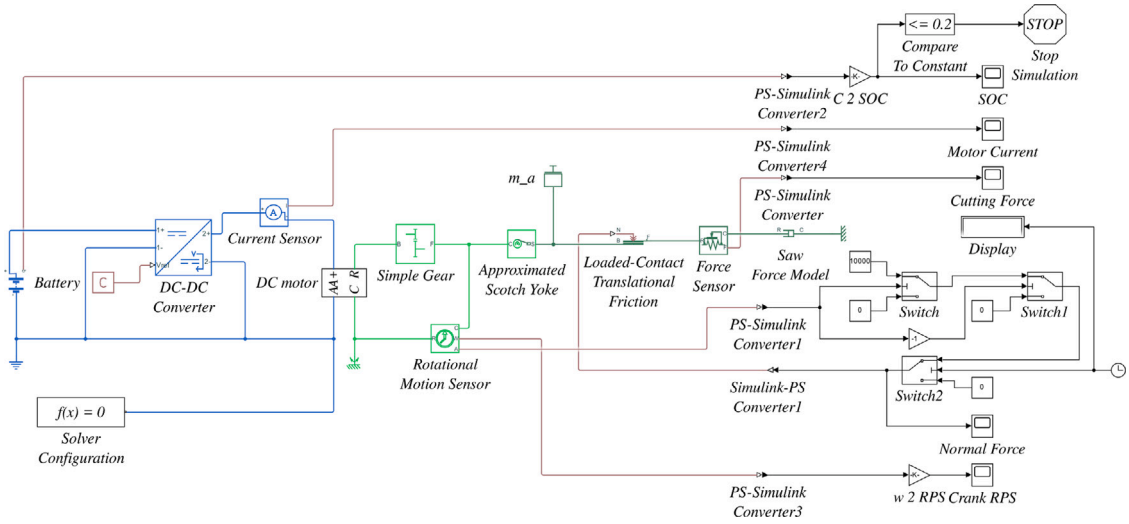

Fig. 11. Battery runtime simulation with a linear cutting force model.

The minimization problem was solved with MATLAB Global Optimization Toolbox, detailed explanation of code can be found in Appendix B.

4.3. Simulation of battery runtime

After the optimization process was completed, additional simulations were performed using the optimal damping factor to estimate the runtime of the jigsaw battery. The models used in these simulations are shown in Figs. 10 and 11.

The two former models and the models presented in Sections 4.1.1 and 4.1.3 are very similar to each other. The only difference is in the modeling of the voltage source and the condition for stopping the simulation. The models presented in Figs. 10 and 11 are detailed Simscape-based simulations of the jigsaw, incorporating not only the dynamics of the cutting process but also the power supply and battery life.

The power source of the system is a battery whose *State of Charge* (SOC) is continuously monitored during the simulation. The current of the battery is regulated by a DC-DC converter, which ensures the appropriate voltage and current supply for the DC motor. This converter is crucial for energy efficiency calculations. Using this block, the actual, PWM controlled input voltage of DC motor is generated as well. Battery behavior is modeled using the *Battery* block, which allows two simulation approaches. If the battery

capacity parameter is set to *Infinite* (*Battery charge capacity: Infinite*), the block models the battery as a series internal resistance and a constant voltage source. This simplified approach is ideal for cases where changes in the battery's State of Charge are not critical. If the battery capacity is defined as finite (*Battery charge capacity: Finite*), the block models the battery as an internal resistance and a voltage source dependent on the state of charge. In this case, the output voltage is calculated using the following equation:

$$V = V_{nom} \frac{\mathrm{SOC}}{1 - \beta(1 - \mathrm{SOC})}, \tag{16}$$

where V_{nom} is the nominal voltage of the battery while SOC denotes the current *State of Charge* of the battery, and β is a parameter describing the internal non-linearity of the battery. This equation accurately models how the battery's output voltage depends not only on the nominal voltage but also on the SOC. As the charge level decreases, the voltage shows a decreasing trend, which is important for energy-efficient operation. This detailed battery model allows the simulation to realistically reflect the dynamics and behavior of a real battery. A unique feature of the models is that they monitor the battery charge level. By continuously monitoring the charge level, the models ensure that the system does not operate if the battery capacity drops to a critical level. If the SOC falls below a predetermined threshold (which is 20%), the model automatically stops the simulation with the help of a logical (*Compare To Constant*) and a stop block (*Stop Simulation*). In the case of a real saw, the aim of this behavior is to protect the battery from damage and ensure safe operation. This feature is particularly important for portable devices, where energy efficiency and battery life are critical considerations. These models are particularly suitable for the development of portable jigsaws, where optimizing energy consumption and improving cutting quality are key objectives. By taking into account the effects of energy consumption on the battery's state of charge, the model allows battery life to be maximized while ensuring stable and reliable system operation. As such, the model is suitable not only for research purposes but also highly applicable to industrial applications, contributing to the advancement of modern jigsaw design and development. The system incorporates multiple sensors that provide real-time data on the system operation. These include the *Current Sensor*, measuring the motor's current draw; the *Force Sensor*, capturing forces in the course of cutting; and the *SOC Monitor*, tracking the battery's charge state and stopping the simulation when critical levels are reached. Logical control elements, such as a *Switch* block, ensure appropriate system state management. For example, the *switch* monitors the SOC and activates the *stop simulation* block if the SOC drops below a set threshold, preventing battery damage while ensuring safe operation. The output of the model includes the cutting force dependent on time and angular position, the current draw of the motor, the SOC, and the angular position and speed of the crank mechanism. These outputs can be visualized in real time or used for further analysis. This model accurately simulates the battery run-time and the dynamics of real cutting force. Considering battery capacity and cutting load, it enables analysis and optimization of energy efficiency. Real cutting data and integrated feedback make this model particularly valuable for the development of portable jigsaws, where improving battery life, energy efficiency, and cutting quality are essential. Under the simulation assumption that the fully charged battery discharges to $20\% SOC$. Battery runtime using the real cutting force model is $t_{br} = 963\,\mathrm{s}$, while using the linear cutting force model is $t_{bl} = 927\,\mathrm{s}$ (detailed explanation in Appendix A).

5. Simulation results

This section presents the results of the investigated simulation results of the study. Fig. 12e provides a detailed comparison of the variation in motor current for both real and linear cutting force models. This figure is a critical result of the paper, as it illustrates the comparison between the two models, highlighting the accuracy of the linear model in approximating the real cutting force. The motor current diagram in the figure shows the real motor current time function ($I_{m,r}(t)$) and the motor current time function generated by the linear model ($I_{m,l}(t)$). The real cutting force current curve is derived from measured data, while the damping factor of the linear model is optimized to minimize the Integral of Squared Errors (ISE), as shown in the identification block diagram. The identification process used the *Simulated Annealing Algorithm* to refine the damping factor (k_{F_c}), ensuring that the linear current curve matches closely the real current curve. Analysis of the motor current diagram reveals that the linear model closely follows the dynamics of the real model, with only minor discrepancies observed in Fig. 12c. The calculated deviations on the motor current between the real and linear cutting force models shown in Fig. 12d. The following equations were calculated to illustrate the deviations:

$$\begin{aligned}
&\delta_{I_m} = I_{m,r} - I_{m,l}, \\
&\left|\delta_{I_m}\right| = \mathrm{abs}\left(\delta_{I_m}\right), \\
&\mathrm{rel}\delta_{I_m} = \frac{I_{m,r} - I_{m,l}}{I_{m,r}}, \\
&\mathrm{rel}\delta_{I_m,\%} = \mathrm{rel}\delta_{I_m} \cdot 100,
\end{aligned} \tag{17}$$

where δ_{I_m} is the motor current deviations. These deviations are minimal, demonstrating that the linear model adequately represents the force effects of the real cutting process. To quantify the difference between the two models by exact value, the Root Mean Square Error (RMSE) calculation can be used to illustrate the difference between the real cutting force model and linear model predictions. The numerical evaluation through this analysis determines the suitability of the linear cutting force model for application. The linearized model proves suitable for battery consumption estimation, since the evaluated value $RMSE = 0.4331\,\mathrm{A}$ supports its practical application for handheld sawing tool runtime prediction. Fig. 12a illustrates the time-dependent variation of the cutting force for both real and linear models and measured cutting force values. This figure is crucial to the study as it highlights the

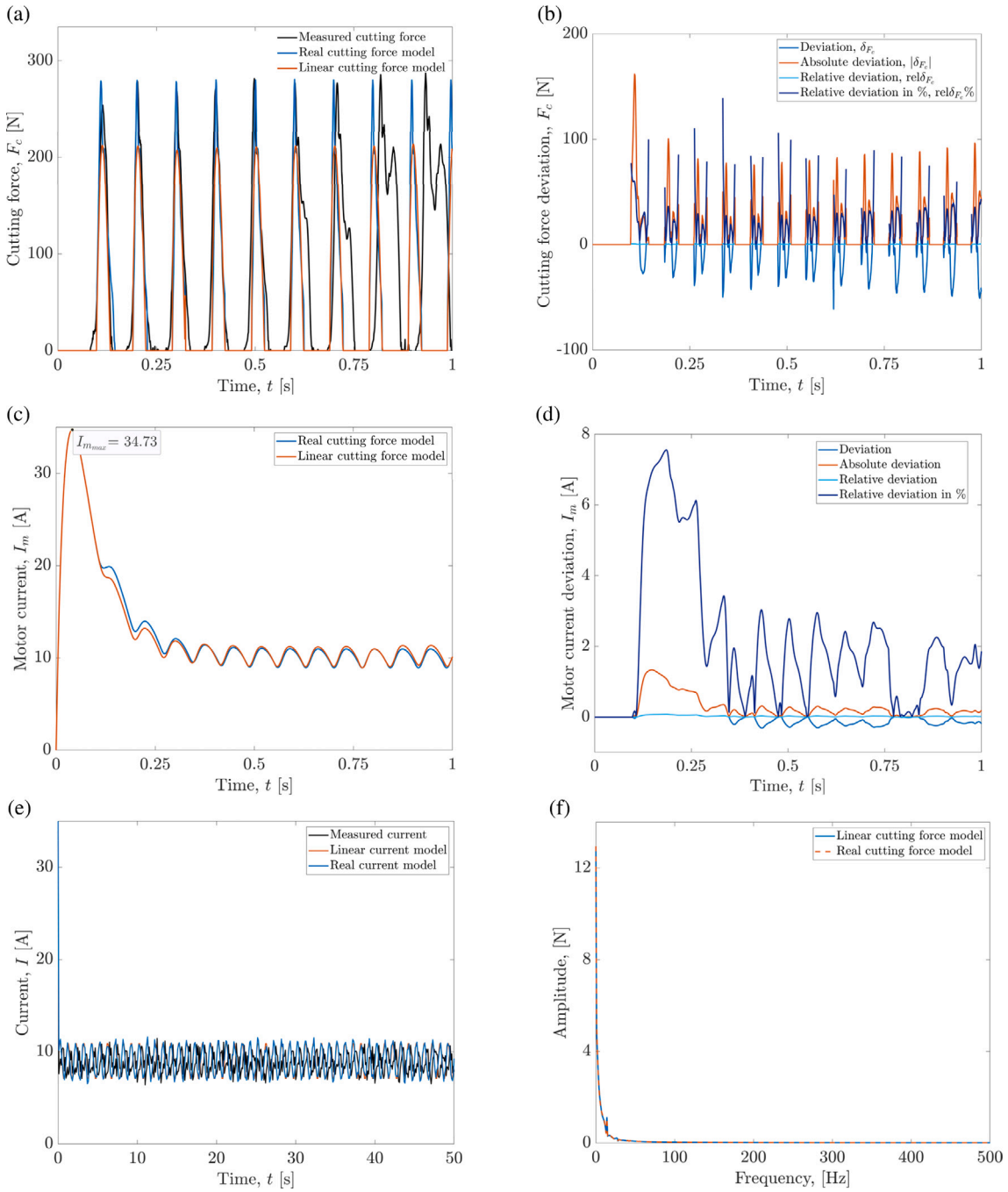

Fig. 12. Simulation results of linear and real cutting force model (a) Measured cutting force and simulated forces on real and linear cutting force models, peak value of cutting force F_c = 280.16 N; (b) Deviations between the real and linear cutting force model results; (c) Motor currents on real and linear cutting force models, peak value of motor current I_m = 34.73 A; (d) Deviations between the real and linear motor models' currents; (e) Comparing the measured motor current and simulated currents on real and linear cutting force models; (f) Comparing the FFT spectrum on real and linear cutting force model.

differences and similarities between the two models and evaluates the linear model's effectiveness in approximating real cutting forces. Deviations on the cutting forces between the real and linear cutting force models were calculated similarly as Eq. (17):

$$\begin{aligned} &\delta_{F_c} = F_{c,r} - F_{c,l}, \\ &\left|\delta_{F_c}\right| = \mathrm{abs}\left(\delta_{F_c}\right), \\ &\mathrm{rel}\delta_{F_c} = \frac{F_{c,r} - F_{c,l}}{F_{c,r}}, \\ &\mathrm{rel}\delta_{F_c,\%} = \mathrm{rel}\delta_{F_c} \cdot 100, \end{aligned} \tag{18}$$

where δ_{F_c} is the deviation of the cutting force between the real and linear cutting force models. The curves in the figure represent the real measured cutting force $\left(F_r(t)\right)$ obtained from direct measurements in the course of jigsaw operation and the simulated cutting force $\left(F_l(t)\right)$ using the linear cutting force model. The parameters of the linear model, particularly the damping factor, were optimized in the course of the identification process to minimize the discrepancies between the real and simulated cutting forces. The identification block diagram forms the basis for the optimization, employing the *Simulated Annealing* algorithm to optimize the damping factor, ensuring that the linear model closely follows the real cutting force.

Analysis of the cutting force-time diagram reveals that the linear model approximates the behavior of the real cutting force, with some deviations observed, especially at force peaks. However, these deviations are negligible compared to the simplicity of the model, and the overall agreement is strong, validating the linear model's applicability in realistic simulations. The optimized linear model effectively captures the force effects and dynamics of the cutting process, providing a reliable estimate of battery runtime under conditions similar to real-world scenarios.

5.1. Current measurement and analysis during cutting force testing

The following section provides a detailed analysis of the cutting force measurement and motor current diagram obtained during the cutting force test (Fig. 12). During the analysis, the average current ($\langle I \rangle$), energy consumption (E), and expected battery runtime $\left(T_{\mathrm{accu}}\right)$ were calculated (see Appendix A). In addition, current fluctuations were thoroughly examined to understand load dynamics during the cutting process better.

A comparison with the linear model was also conducted to highlight differences between real-world measurements and simulated predictions. The diagram shown in Fig. 12e shows that the simulated and measured current-time $I(t)$ curves fit well with each other, the main dynamic characteristics (amplitude, trend, period) are nearly identical. The maximum current corresponds to periods of high cutting resistance, whereas the minimum current reflects load reductions during lighter cutting phases or pauses. The diagram's characteristic waveform reveals the cutting process's repetitive and dynamic nature. Detailed analysis of the current-time diagram highlights the following features.

(1) The oscillation period is approximately $0.1\,\mathrm{s}$, corresponding to the cyclic dynamics of the cutting process.
(2) Rapid current increases are observed during higher cutting resistance, indicating the motor's response to the increased load.
(3) The main frequency components of the curves of the real and linear cutting force model coincide well. This indicates that the model behaves reliably not only in time, but also in the periodic nature of the cutting force.

6. Conclusions

Based on the analyses and results, the model and simulation evaluations presented in this paper accurately reflect the essential dynamic characteristics of the jigsaw operation and provide a clear representation of the relationship between the real and linear models. The electromechanical model implemented in Simscape utilizes real data and simulates the cutting process through the fundamental operation of the DC motor and the Scotch yoke mechanism. The physical elements provided by the Simscape modeling environment, combined with its integration with Simulink, enable detailed representation of both electrical and mechanical properties, enhancing realism.

(1) The efficiency of the identification block diagram and the Simulated Annealing algorithm used in the optimization process is demonstrated by the sufficiently accurate approximations of the motor current and cutting force-time functions. The block diagram's logic minimizes differences between measured and simulated values by ensuring the linear model closely resembles real-world behavior. With a relative inaccuracy of 3.7% on battery capacity compared to actual data, the linear damping factor optimization produces a very effective linear model that accurately depicts the cutting force behavior.
(2) The analysis of the motor current-time and cutting force-time diagrams indicates that the linear model approximation offers a practical, fast-running alternative to the complex real system. Despite its simplicity, the optimized linear model can estimate battery run-time with surprising accuracy and dynamic force effects of the cutting process, enabling reliable predictions.
(3) The results suggest that the models presented, the optimization process, and the Simscape-based simulations provide an effective tool for an accurate but computationally efficient approximation of electromechanical systems.

While the linearized model demonstrates strong performance within the calibrated operating conditions, it is important to acknowledge its limitations when extrapolating to longer-term or highly nonlinear scenarios. Factors such as progressive tool wear, changes in blade stiffness, and vibration-induced harmonics can gradually deviate the system behavior from the idealized assumptions. These nonlinear effects may alter the dynamic force signature and motor loading pattern over time, potentially impacting runtime prediction accuracy. Although such effects were not the primary focus of this study, future extensions could incorporate wear progression models, harmonic analysis, or adaptive parameter updating schemes to enhance long-term robustness and reliability.

The methodology applied here is not limited to jigsaws; however, it can be extended to other systems characterized by cyclic force effects, where precise simulation and performance estimation are critical.

CRediT authorship contribution statement

Sándor Apáti: Writing – review & editing, Writing – original draft, Validation, Data curation. **György Hegedűs:** Writing – review & editing, Visualization, Supervision, Project administration. **Sándor Hajdu:** Writing – original draft, Methodology, Formal analysis, Conceptualization.

Declaration of competing interest

The authors declare the following financial interests/personal relationships which may be considered as potential competing interests: Gyorgy Hegedus reports was provided by University of Miskolc. If there are other authors, they declare that they have no known competing financial interests or personal relationships that could have appeared to influence the work reported in this paper.

Appendix A. Validation based on the 50-s interval

To evaluate the reliability of the simulation model, the expected battery runtime was calculated not only over the full test duration, but also for a representative 50-s interval that aligns with the actual measurement data. This interval adequately reflects the system's loading conditions and the periodic behavior of both the motor current and the cutting force, making it suitable for validating the model's accuracy.

Based on the measurement and simulation data, the following average current values were obtained:

– From real measurements:

$$\langle I_{\text{measured}} \rangle = 8.51\,\text{A},$$

– From the fitted linear model:

$$\langle I_{\text{lin}} \rangle = 7.77\,\text{A},$$

– From the nonlinear model:

$$\langle I_{\text{nonlin}} \rangle = 8.24\,\text{A}.$$

The battery's total charge is $Q = 2.5\,\text{Ah} = 9000\,\text{As}$. As the simulation assumes a discharge from 100% down to 20% SOC, the usable charge is:

$$Q_{\text{usable}} = 9000\,\text{A s} \cdot 0.8 = 7200\,\text{A s}. \tag{A.1}$$

The expected battery runtime can be calculated using the following formula:

$$T = \frac{Q_{\text{usable}}}{\langle I \rangle}. \tag{A.2}$$

Applying this equation yields the following runtimes for each case:

$$T_{\text{measured}} = \frac{7200\,\text{A s}}{8.51\,\text{A}} \approx 846.0\,\text{s}, \tag{A.3}$$

$$T_{\text{lin}} = \frac{7200\,\text{A s}}{7.77\,\text{A}} \approx 926.96\,\text{s}, \tag{A.4}$$

$$T_{\text{nonlin}} = \frac{7200\,\text{A s}}{8.24\,\text{A}} \approx 873.8\,\text{s}. \tag{A.5}$$

The relative deviation of the linear model compared to the measured runtime is:

$$\Delta_{\text{lin}} = \frac{926.96\,\text{s} - 846.0\,\text{s}}{846.0\,\text{s}} \cdot 100 \approx 9.6\%. \tag{A.6}$$

For the nonlinear model:

$$\Delta_{\text{nonlin}} = \frac{873.8\,\text{s} - 846.0\,\text{s}}{846.0\,\text{s}} \cdot 100 \approx 3.3\%. \tag{A.7}$$

These results demonstrate that the nonlinear model provides a very close match to the measured values, while the simpler linear model — despite its approximative nature — also yields sufficiently accurate estimates. The relative deviations between 3.3% and 9.6% confirm the applicability of both models for predicting battery energy consumption in industrial simulation and design tasks.

Appendix B. Simulated annealing algorithm - MATLAB code

```
%-------------------------------------------------------------%
% Linear parameter identification of jigsaw cutting force %
% based on optimization                                      %
% using Matlab function (Simulated cooling algorithm)     %
%-------------------------------------------------------------%
% Load input parameters to MATLAB workspace (see Table 3):
J_m=2.4e-5;   % Moment of inertia of DC motor  [kgm^2]
J_c=2.38e-5;  % Moment of inertia of Yoke wheel [kgm^2]
k_mc=6/56;    % Reciprocal of the gear ratio [-]
r_c=0.01;     % Eccentricity [m]
m_a= 0.239;   % Mass of moving components [kg]
L=3.21e-3;    % Coil inductance [H]
R=0.176;      % Circuit resistance [Ohm]
k_e=7.383e-3; % Motor electricconstant [Vs/rad]
k_m=5.632e-3; % Motor torque constant [Nm/A]
n_em=42.08;   % Eccenter max. speed [1/s]
n_ea=18.41;   % Eccenter current speed [1/s]
PWM=n_ea/n_em;% PWM duty cycle [%]
U_0=18;       % Battery voltage [V]
U_m=U_0*PWM;  % Motor terminal voltage [V]
Q_b=1.5;      % Battery capacity [Ah]
b=3.4274e-6;  % Internal damping coefficient [Nms/rad]

% Loading the effective cutting force vs. eccentric angle relationship
load('Impulse_cutting_force',"Fc_eff_fi")

% Linear cutting force parameter (damping factor) [Ns/m]:
d_Fc=100;

% The optimal value of the linear cutting force parameter (damping factor)
% [Ns/m]:
d_Fc_opt=240.29;

% Open Simulink models:
open('Jigsaw_linear_ident.slx');
open('Jigsaw_real_ident.slx');

% Performing the simulation of real model
% in order to get the 'Motor_current_real' array:
sim('Jigsaw_real_ident.slx');

% Optimization parameters:
fun=@objfunc4optimSA; % Objective function
d_init=130; % Initial value of parameter
d_l=100; % Lower bound of parameter
d_u=500; % Upper bound of parameter

% Plotting options:
options = optimoptions(@simulannealbnd, ...
'PlotFcn',{@saplotbestf,@saplottemperature,@saplotf,@saplotstopping});

% Running optimization:
[d_opt,~,exitFlag,output] = simulannealbnd(fun,d_init,d_l,d_u,options);

% Printing results:
```

```
fprintf('Number of iterations : %d\n', output.iterations);
fprintf('Optimal damping value : %d\n', d_opt);

function f_out=objfunc4optimSA(dvar)
% Calculating the value of objective function for the
% jigsaw cutting force linear parameter optimization task
%
% Function syntax with flexible input parameter set:
% f_out=objfunc4optimSA(dvar)
%
% dvar(1) = Cutting force parameter (linear damping) [100..500]
%
% The function output equals the integral squared error (ISE)
% of motor current functions for real and linear model simulations

% Assigning the value of input parameter to the workspace variable:
assignin('base','d_Fc',dvar(1));

% Performing the simulation of linear model
% in order to get the 'Motor_current_linear' array:
Simres=sim('Jigsaw_linear_ident.slx');

% Determining the current vector of linear and real model simulations:
linear_current=Simres.Motor_current_linear;
real_current=evalin('base','Motor_current_real');

% Calculating the output value:
val_ISE=0;
for i=1:length(real_current)
    err=(real_current(i)-linear_current(i))^2;
    val_ISE=val_ISE+err;
end
f_out=val_ISE;
end % of function
```

Data availability

No data was used for the research described in the article.

References

[1] H. Ioras, T. Nicholls, M.C. Perkins, U.V. Münz, A. Larmann, A review for cutting forces and stresses in circular saws, Eur. J. Wood Wood Prod. 60 (1) (2002) 55–59, http://dx.doi.org/10.1007/S001070100220.

[2] B. Porankiewicz, B. Axelsson, A. Grönlund, B. Marklund, Main and normal cutting forces by machining wood of pinus sylvestris, Bioresour. 6 (4) (2011) 3687–3713, http://dx.doi.org/10.15376/BIORES.6.4.3687-3713.

[3] B. Porankiewicz, G. Goli, Cutting forces by oak and douglas fir machining, Maderas Ciencia Tecnol. 16 (2) (2014) 199–216, URL.

[4] L. Cristovao, O. Broman, A. Grönlund, M. Ekevad, R. Sitoe, Main cutting force models for two species of tropical wood, Wood Mater. Sci. Eng. 7 (3) (2012) 143–149, http://dx.doi.org/10.1080/17480272.2012.662996.

[5] D. Germain, G. Fromentin, G. Poulachon, S. Bissey-Breton, From large-scale to micromachining: A review of force prediction models, J. Manuf. Process. 15 (3) (2013) 389–401, http://dx.doi.org/10.1016/J.JMAPRO.2013.02.006.

[6] B. Denkena, J. Vehmeyer, D. Niederwestberg, P. Maaß, Identification of the specific cutting force for geometrically defined cutting edges and varying cutting conditions, Int. J. Mach. Tools Manuf. 82 (2014) 42–49, http://dx.doi.org/10.1016/J.IJMACHTOOLS.2014.03.009.

[7] P. Kolar, P. Fojtu, T.L. Schmitz, On cutting force coefficient model with respect to tool geometry and tool wear, Procedia Manuf. 1 (2015) 708–720, http://dx.doi.org/10.1016/J.PROMFG.2015.09.020.

[8] T. Krenke, S. Frybort, U. Müller, Cutting force analysis of a linear cutting process of spruce, Wood Mater. Sci. Eng. 13 (5) (2018) 279–285, http://dx.doi.org/10.1080/17480272.2017.1324916.

[9] W. Li, Z. Zhang, B. Luo, Effects of sawtooth side edges with different radial clearance angles on the cutting force in wood sawing, Mater. Und Werkst. 49 (12) (2018) 1468–1475, http://dx.doi.org/10.1002/MAWE.201800074.

[10] R. Curti, B. Marcon, L. Denaud, M. Togni, R. Furferi, G. Goli, Generalized cutting force model for peripheral milling of wood, based on the effect of density, uncut chip cross section, grain orientation and tool helix angle, Eur. J. Wood Wood Prod. 79 (3) (2021) 667–678, http://dx.doi.org/10.1007/S00107-021-01667-5.

[11] M. Torkghashghaei, W. Shaffer, R. Georges, B. Ugulino, R.E. Hernández, C. Blais, Effect of variable engineered micro-geometry of the cutting edges of circular saws on the surface quality of SPF boards, Eur. J. Wood Wood Prod. 81 (5) (2023) 1261–1276, http://dx.doi.org/10.1007/s00107-023-01961-4.

[12] A. Jaquemod, K. Güzel, H.-C. Möhring, Influence of minimum quantity lubrication on tool temperature and wear in wood machining, in: Production At the Leading Edge of Technology, Springer Nature Switzerland, 2023, pp. 717–726, http://dx.doi.org/10.1007/978-3-031-47394-4_70, Chapter Environmentally Neutral Production.

[13] F. Schreiner, M. Beller, J. Pohle, B. Thorenz, F. Döpper, Life cycle assessment (LCA) of a circular saw blade for wood processing, in: Sustainable Manufacturing As a Driver for Growth, Springer Nature Switzerland, 2025, pp. 155–164, http://dx.doi.org/10.1007/978-3-031-77429-4_18, Chapter Life Cycle Thinking.
[14] Y. Huang, D. Chuchala, D. Buck, K.A. Orlowski, M. Fredriksson, M. Svensson, Analysis of the relationship between cutting forces and local structural properties of scots pine wood aided by computed tomography, Int. J. Adv. Manuf. Technol. 135 (9–10) (2024) 4975–4987, http://dx.doi.org/10.1007/s00170-024-14797-w.
[15] M.D. Mandić, B. Porankiewicz, G.J. Danon, An attempt at modelling of cutting forces in oak peripheral milling, Bioresour. 10 (3) (2015) http://dx.doi.org/10.15376/biores.10.3.5489-5502.
[16] P. Moradpour, K. Doosthoseini, F. Scholz, A. Tarmian, Cutting forces in bandsaw processing of oak and beech wood as affected by wood moisture content and cutting directions, Eur. J. Wood Wood Prod. 71 (6) (2013) 747–754, http://dx.doi.org/10.1007/s00107-013-0734-z.
[17] K.A. Orlowski, T. Ochrymiuk, A. Atkins, D. Chuchala, Application of fracture mechanics for energetic effects predictions while wood sawing, Wood Sci. Technol. 47 (5) (2013) 949–963, http://dx.doi.org/10.1007/s00226-013-0551-x.
[18] K. Orłowski, T. Ochrymiuk, A.G. Atkins, An innovative approach to the forecasting of energetic effects while wood sawing, Drv. Ind. 65 (4) (2014) 273–281, http://dx.doi.org/10.5552/DRIND.2014.1341.
[19] K. Orłowski, T. Ochrymiuk, A newly-developed model for predicting cutting power during wood sawing with circular saw blades, Maderas Ciencia Tecnol. 19 (2) (2017) 149–162, http://dx.doi.org/10.4067/S0718-221X2017005000013.
[20] L. Hlásková, K. Orłowski, Z. Kopecký, M. Jedinák, Sawing processes as a way of determining fracture toughness and shear yield stresses of wood, Bioresour. 10 (3) (2015) 5381–5394, http://dx.doi.org/10.15376/BIORES.10.3.5381-5394.
[21] L. Hlásková, Z. Kopecký, V. Novák, Influence of wood modification on cutting force, specific cutting resistance and fracture parameters during the sawing process using circular sawing machine, Eur. J. Wood Wood Prod. 78 (6) (2020) 1173–1182, http://dx.doi.org/10.1007/S00107-020-01581-2.
[22] J.-P. Costes, P.L. Ko, T. Ji, C. Decès-Petit, Y. Altintas, Orthogonal cutting mechanics of maple: modeling a solid wood-cutting process, J. Wood Sci. 50 (1) (2004) 28–34, http://dx.doi.org/10.1007/S10086-003-0527-9.
[23] Y. Luo, Y. Ren, Y. Ren, Z. Zhou, X. Huang, T. Song, Prediction of single-tooth sawing force based on tooth profile parameters, Int. J. Adv. Manuf. Technol. 86 (1) (2016) 641–650, http://dx.doi.org/10.1007/S00170-015-8201-0.
[24] K. Orłowski, T. Ochrymiuk, L. Hlaskova, D. Chuchala, Z. Kopecky, Revisiting the estimation of cutting power with different energetic methods while sawing soft and hard woods on the circular sawing machine: a central European case, Wood Sci. Technol. 54 (2) (2020) 457–477, http://dx.doi.org/10.1007/S00226-020-01162-9.
[25] M. Khelifa, A. Khennane, Numerical analysis of the cutting forces in timber, J. Eng. Mech. Asce 140 (3) (2014) 523–530, http://dx.doi.org/10.1061/(ASCE)EM.1943-7889.0000671.
[26] R. Marchal, F. Mothe, L.-E. Denaud, B. Thibaut, L. Bleron, Cutting forces in wood machining – basics and applications in industrial processes. a review COST action E35 2004–2008: Wood machining – micromechanics and fracture, Holzforschung 63 (2) (2009) 157–167, http://dx.doi.org/10.1515/HF.2009.014.
[27] A. Naylor, P. Hackney, N. Perera, E. Clahr, A predictive model for the cutting force in wood machining developed using mechanical properties, Bioresour. 7 (3) (2012) 2883–2894, http://dx.doi.org/10.15376/BIORES.7.3.2883-2894.
[28] M. Conward, J. Samuel, A microstructure-based mechanistic model for bone sawing: Part 1—Cutting force predictions, J. Manuf. Sci. Eng. Trans. Asme 143 (12) (2021) 1–19, http://dx.doi.org/10.1115/1.4051236.
[29] R. Mishra, M. Conward, J. Samuel, A microstructure-based mechanistic model for bone sawing: Part 2—Acoustic energy rate predictions, J. Manuf. Sci. Eng. 143 (12) (2021) 121010, http://dx.doi.org/10.1115/1.4051237.
[30] J. Kang, J. Zhang, Z. Duan, H. Zhang, Modeling for prediction of sawing force based on the maximum undeformed chip distribution in the granite sawing, Int. J. Adv. Manuf. Technol. 124 (1–2) (2022) 111–126, http://dx.doi.org/10.1007/s00170-022-10479-7.
[31] X. Xu, Research on cutting force based on thermal-mechanical coupling precision modeling, Sci. J. Technol. 4 (5) (2022) 25–31, http://dx.doi.org/10.54691/sjt.v4i5.754.
[32] M. Yu, B. Wang, P. Ji, B. Li, L. Zhang, Q. Zhang, Simulation analysis of the circular sawing process of medium density fiberboard (MDF) based on the Johnson–Cook model, Eur. J. Wood Wood Prod. 82 (2) (2023) 447–459, http://dx.doi.org/10.1007/s00107-023-02007-5.
[33] P. Ni, Y. Wang (CA), D. Tan, Y. Zhang, Z. Chen, Z. Wang, C. Yi, L. Shao, Y. Lu, Research on optimization method of stainless steel sawing process parameters based on multi-tooth sawing force prediction model, Int. J. Adv. Manuf. Technol. 128 (9) (2023) 4513–4533, http://dx.doi.org/10.1007/s00170-023-12051-3.
[34] J. Ni, L. Li, M.S.H. Al-Furjan, J. Xu, X. Yang, Establishment and verification of a dynamic cutting force model for metal bandsawing, Int. J. Adv. Manuf. Technol. 90 (2017) 2703–2712, http://dx.doi.org/10.1007/s00170-016-9568-2.
[35] N. Vorkapic, N. Slavkovic, B. Kokotovic, S. Zivanovic, Z. Dimic, Implementation of a cutting forces model through virtual simulation of machining process, Int. J. Adv. Manuf. Technol. 135 (2024) 3085–3099, http://dx.doi.org/10.1007/s00170-024-14681-7.
[36] P. Pichler, M. Leitner, F. Grün, C. Guster, Evaluation of wood material models for the numerical assessment of cutting forces in chipping processes, Wood Sci. Technol. 52 (1) (2018) 281–294, http://dx.doi.org/10.1007/S00226-017-0962-1.
[37] W. Huang, H. Chen, Q. Jin, J. Shi, X. Guo, B. Na, Prediction of milling performance of thermally modified wood based on machine learning, Eur. J. Wood Wood Prod. 83 (2) (2025) http://dx.doi.org/10.1007/s00107-025-02224-0.
[38] M. Derbas, A. Jaquemod, S. Frömel-Frybort, K. Güzel, H.-C. Moehring, M. Riegler, A machine learning approach to predict properties of wood products during milling, For. Prod. J. 74 (S2) (2024) 1–8, http://dx.doi.org/10.13073/fpj-d-24-00012.
[39] Z. Lai, H. Huang, Z. Hu, X.J. Liao, Dynamic model and machining mechanism of wire sawing, J. Mater. Process. Technol. 311 (2022) 117820, http://dx.doi.org/10.1016/j.jmatprotec.2022.117820.
[40] J. Sandak, K. Orłowski, T. Ochrymiuk, A. Sandak, M. Riggio, An alternative way of determining mechanical properties of wood by measuring cutting forces, in: Proceedings of the International Conference on Structural Health Assessment of Timber Structures, SHATIS'15, 2015, pp. 543–551.
[41] B. Zhang, C. Zhao, B. Wen, Dynamic cutting force measurement test and prediction of time series model for machine tools, J. Northeast. Univ. (Nat. Sci.) 40 (4) (2019) 521–526, http://dx.doi.org/10.12068/j.issn.1005-3026.2019.04.013.
[42] V. Nasir, J. Cool, Intelligent wood machining monitoring using vibration signals combined with self-organizing maps for automatic feature selection, Int. J. Adv. Manuf. Technol. 108 (5) (2020) 1811–1825, http://dx.doi.org/10.1007/s00170-020-05505-5.
[43] T. Thaler, P. Potočnik, I. Bric, E. Govekar, Chatter detection in band sawing based on discriminant analysis of sound features, Appl. Acoust. 77 (2014) 114–121, http://dx.doi.org/10.1016/j.apacoust.2012.12.004.
[44] V. Meulenberg, M. Ekevad, M. Svensson, O. Broman, Minor cutting edge force contribution in wood bandsawing, J. Wood Sci. 68 (1) (2022) http://dx.doi.org/10.1186/s10086-022-02023-8.
[45] P. McDonald, Investigation of cutting force and surface quality in Frozen wood sawing under varying influencing factors to improve the energy- and resource efficiency of sawing processes, in: Manufacturing Driving Circular Economy, Springer eBooks, 2023, pp. 166–174, http://dx.doi.org/10.1007/978-3-031-28839-5_19.
[46] L. Kazup, A. Váradine Szarka, Cutting force measurement of electrical jigsaw by strain gauges, J. Phys. Conf. Ser. 772 (2016) 012030, http://dx.doi.org/10.1088/1742-6596/772/1/012030.

[47] M.A. Blokhin, I.I. Dymchakov, A.P. Shein, D.D. Emel'yanov, Dynamic control of the resonant frequency of the blade of the saw module performing a circular flat rotational–translational motion, J. Mach. Manuf. Reliab. 53 (7) (2024) 799–806, http://dx.doi.org/10.1134/s1052618824700572.
[48] C. Marega, M. Ghellere, S. Grigolato, R. Cavalli, Sensor-integrated saw blade monitoring for cutting stability, Appl. Sci. 14 (11) (2024) 4730, http://dx.doi.org/10.3390/app14114730.
[49] Z. Zhang, J. Li, B. He, Y. Feng, AI-enhanced wear monitoring for wire sawing of hard materials, Expert Syst. Appl. 235 (2025) 127446, http://dx.doi.org/10.1016/j.eswa.2025.127446.
[50] M. Yu, H. Liu, F. Yang, L. Zhang, Y. Wang, A deep learning-enabled digital twin for tool condition monitoring in milling, J. Intell. Manuf. (2024) http://dx.doi.org/10.1007/s10845-023-02260-8.
[51] X. Sun, H. Li, Z. Wang, Y. Liu, Path planning and force control of intelligent milling process via DRL, Expert Syst. Appl. 235 (2025) 127471, http://dx.doi.org/10.1016/j.eswa.2025.127471.
[52] M. Derbas, A. Jaquemod, S. Frömel-Frybort, K. Güzel, H.-C. Moehring, M. Riegler, A machine learning approach to predict properties of wood products during milling, For. Prod. J. 74 (S2) (2024) 1–8, http://dx.doi.org/10.13073/FPJ-D-24-00012, URL https://www.doi.org/10.13073/FPJ-D-24-00012.
[53] S. Apáti, G. Hegedűs, S. Hajdu, Semi-in-situ cutting force measurement of a jigsaw, Results Eng. 25 (2025) 104114, http://dx.doi.org/10.1016/j.rineng.2025.104114.
[54] L. Zhang, R. Zhang, L. Xie, S. Xue, Dynamics and isolation performance of a vibration isolator with a yoke-type nonlinear inerter, Int. J. Mech. Sci. 254 (2023) 108447, http://dx.doi.org/10.1016/j.ijmecsci.2023.108447.
[55] S. Jia, C. Hong, G. Shi, J. Han, R. Xu, Y. Xia, H. Xia, Scotch yoke structure inspired piezoelectric-electromagnetic hybrid harvester for wave energy harvesting, J. Intell. Mater. Syst. Struct. 35 (20) (2024) 1540–1557, http://dx.doi.org/10.1177/1045389x241283121.
[56] S. Lin, J. Ma, J. Li, S. Li, M. Wang, Y. Hu, J. Wen, A novel inertial impact piezoelectric actuator with adjustable angle vibrators, Int. J. Mech. Sci. 244 (2023) 108071, http://dx.doi.org/10.1016/j.ijmecsci.2022.108071.
[57] Y. Hu, Y. Hu, S. Lin, J. Ma, S. Li, J. Li, J. Wen, Theoretical modeling and dynamic characteristics analysis of piezoelectric inertial actuator, Int. J. Mech. Sci. 225 (2022) 107363, http://dx.doi.org/10.1016/j.ijmecsci.2022.107363.
[58] R. Wang, F. Huang, H. Huang, J. Chen, Configuration synthesis and screening method for multiple closed-loop unit tandem mechanisms, Mech. Mach. Theory 202 (2024) 105770, http://dx.doi.org/10.1016/j.mechmachtheory.2024.105770.